

Pulse time reversal and stopping by a refractive index front


Cite as: APL Photonics 5, 080801 (2020); <https://doi.org/10.1063/5.0007986>

Submitted: 18 March 2020 . Accepted: 03 July 2020 . Published Online: 14 August 2020

Mahmoud A. Gaafar , Jannik Holtorf, Manfred Eich, and Alexander Yu. Petrov

COLLECTIONS

 This paper was selected as Featured

 This paper was selected as Scilight



View Online



Export Citation



CrossMark

ARTICLES YOU MAY BE INTERESTED IN

[Determining the refractive index of shocked \[100\] lithium fluoride to the limit of transmissibility](#)


Journal of Applied Physics **116**, 033515 (2014); <https://doi.org/10.1063/1.4890714>

[Experimental demonstration of negative index of refraction](#)

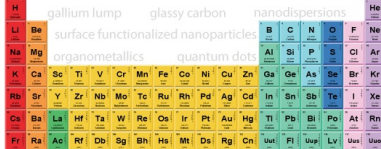
Applied Physics Letters **88**, 221103 (2006); <https://doi.org/10.1063/1.2208264>

[Ordinary refractive index of sapphire in uniaxial tension and compression along the c axis](#)

Journal of Applied Physics **93**, 1023 (2003); <https://doi.org/10.1063/1.1530716>



THE ADVANCED MATERIALS MANUFACTURER®



additive manufacturing epitaxial crystal growth cerium oxide polishing powder silver nanoparticles sputtering targets III-IV semiconductors CVD precursors europium phosphors

deposition slugs OLED Lighting spintronics solar energy osmium nanoribbons thin films chalcogenides AuNPs GDC Li-ion battery electrolytes 99.999% ruthenium spheres

endohedral fullerenes copper nanoparticles diamond micropowder CIGS MBE grade materials palladium catalysts flexible electronics beta-barium borate borosilicate glass dysprosium pellets YBCO pyrolytic graphite 3d graphene foam indium tin oxide mesoporous silica raman substrates sapphire windows tungsten carbide InGaAs barium fluoride carbon nanotubes lithium niobate scandium powder

gallium lump glassy carbon nanodispersions surface functionalized nanoparticles organometallics quantum dot

Al Si P S Cl Ar B C N O F Ne Ga Ge As Se Br Kr Ti Zr Nb Mo Ta Ru Rh Pd Ag Cd In Sn Sb Te I Xe Hf Ta W Re Os Ir Pt Au Hg Tl Pb Bi Po At Rn

perovskite crystals yttrium iron garnet alternative energy h-BN fused quartz metalocenes platinum ink buckyballs Ti-6Al-4V rhodium sponge fiber optics beamsplitters infrared dyes zeolites

Now Invent.
The Next Generation of Material Science Catalogs

American Elements opens up a world of possibilities so you can **Now Invent!**

Over 15,000 certified high purity laboratory chemicals, metals, & advanced materials and a state-of-the-art Research Center. Printable GHS-compliant Safety Data Sheets. Thousands of new products. And much more. All on a secure multi-language "Mobile Responsive" platform.

www.americanelements.com

Pulse time reversal and stopping by a refractive index front

Cite as: APL Photon. 5, 080801 (2020); doi: 10.1063/5.0007986

Submitted: 18 March 2020 • Accepted: 3 July 2020 •

Published Online: 14 August 2020



Mahmoud A. Gaafar,^{1,2,a)}  Jannik Holtorf,¹ Manfred Eich,^{1,3} and Alexander Yu. Petrov^{1,4}

AFFILIATIONS

¹Institute of Optical and Electronic Materials, Hamburg University of Technology, Eissendorfer Strasse 38, 21073 Hamburg, Germany

²Department of Physics, Faculty of Science, Menoufia University, Menoufia, Egypt

³Institute of Materials Research, Helmholtz-Zentrum Geesthacht, Max-Planck-Strasse 1, Geesthacht D-21502, Germany

⁴ITMO University, 49 Kronverkskii Ave., 197101 St. Petersburg, Russia

^{a)}Author to whom correspondence should be addressed: mahmoud.gaafar@tuhh.de

ABSTRACT

We discuss how dynamic light stopping and pulse time reversal can be implemented in dispersive waveguides via indirect photonic transitions induced by moving refractive index fronts. The previous concepts of light stopping/time reversal either require complex local variation of the device's refractive index or rely on the strict phase matching condition, which imposes limitations on the amount of manipulated information. Until now, only single pulses or continuous waves were manipulated experimentally. Our scheme is not limited by a strict phase matching condition and does not require local index variations, thus it can manipulate broadband signals in a single step process. Here, we present several numerically integrated results for pulse time reversal and stopping/storage via indirect front-induced transitions. The presented results are experimentally feasible using existing photonic waveguide technologies.

© 2020 Author(s). All article content, except where otherwise noted, is licensed under a Creative Commons Attribution (CC BY) license (<http://creativecommons.org/licenses/by/4.0/>). <https://doi.org/10.1063/5.0007986>

I. INTRODUCTION

Dynamic control of optical pulse propagation in dispersive waveguides has potential applications in many fields, such as signal processing,¹ optical,¹ and quantum communications.² For instance, the time reversal of light pulses,^{3–6} which means that the time order of the incident light is reversed, can be used to send information back, compensating the additional phase distortions in the transmission system. Several experimental studies on the time reversal of light have been based on nonlinear processes, such as three-wave or four-wave mixing systems.^{3,4} However, the ability to reverse pulses with a broadband spectrum is limited due to the phase-mismatching problem. These approaches require exact group velocity and/or phase velocity matching of pump, signal, and idler waves. On the other hand, dynamic schemes, where refractive index changes during the signal propagation, can provide a time reversal of light with wide-bandwidth operation.^{7–10} Time reversal schemes were proposed based on the adiabatic^{5–7} and non-adiabatic⁹ reversal of

the mode group velocity or on Bloch oscillations in a dynamically chirped coupled resonator waveguide.⁸ We should mention that none of these schemes have been realized experimentally in the optical regime so far. Recently, Konoike *et al.* demonstrated experimentally a dynamic time reversal of light oscillation inside a system of three coupled cavities.¹¹ Such a system can be considered as a building block for a coupled cavity waveguide. However, switching of the packet of information in such a waveguide would require thermal tuning of each of the cavities and fast dynamic switching of each second cavity in the waveguide, which is difficult to realize.

A similar topic is the dynamic light stopping, where the slope of the dispersion relation is not reversed but flattened.^{12–15} Stopping offers new possibilities in enhanced light-matter interactions and all-optical processing, such as optical buffering.^{16,17} Light storage and release by direct transition, when light experiences frequency change only, in photonic waveguides has been theoretically proposed by Yanik *et al.*^{12,18} In this case, the dispersion relation is modified to have a zero slope in a switched state and the signal

bandwidth ideally collapses to a single frequency. To release the signal, the system should be switched back to the original dispersion relation. However, such a strong modification of the dispersion relation, similar to time reversal, requires fast and strong local refractive index changes^{18,19} that are difficult to achieve.¹⁴ Thus, several studies experimentally demonstrated similar operation by controlling the Q factor in a single cavity or two coupled cavities.^{20–24} However, the limitation of the dynamic storage in the cavity is the amount of stored information. Namely, a single pulse can be stored but not a sequence of pulses.

On the other hand, light manipulation in waveguides by a moving refractive index front has caught the attention in recent years.^{25–38} In this case, the ratio of the signal frequency change $\Delta\omega$ and wavenumber change $\Delta\beta$ induced by the interaction with the moving front is equal to the group velocity of the front, i.e., $\Delta\omega/\Delta\beta = v_f$. Therefore, the angle of this kind of indirect transition within the dispersion diagram is defined by the front velocity v_f .^{25,30} In contrast to direct transitions in which the signal frequency changes while its wavenumber stays the same, indirect transitions create an additional method for frequency and wavenumber control via the choice of the transition angle. Therefore, there is no need to strongly modify or flatten the dispersion relation to reverse or stop the light. By an indirect transition, the initial state can be projected to the part of the dispersion relation with the required slope. In this regard, the front-induced time-reversal and pulse stopping schemes provide a single platform that can implement both frequency conversion and time reversal/pulse stopping of arbitrary envelopes at the same time, which will be useful for major applications in the future optical communication systems.

In this paper, we present several numerically simulated results for pulse time reversal and light stopping/storage via indirect front induced transitions (FITs) and compare the obtained results to theoretical predictions. We also discuss how to realize these effects in real systems.

II. METHOD

The temporal evolution of a signal envelope function $A(t, z)$ in a dispersive waveguide with an index front described by the dispersion relation shift in space and time $\Delta\omega_D(t, z)$ can be modeled with the slowly varying envelope (SVE) approximation with the carrier angular frequency ω_0 and carrier wavenumber β_0 as follows:³⁹

$$\frac{\partial A(t, z')}{\partial t} = (v_f - v_{g0}) \frac{\partial A}{\partial z'} + \sum_{n=2}^N i^{n+1} \frac{\omega_n}{n!} \frac{\partial^n A}{\partial z'^n} + i\Delta\omega_D(z')A. \quad (1)$$

Here, v_{g0} is the group velocity at β_0 , $\omega_n = \partial^n \omega / \partial \beta^n$ are the dispersion coefficients associated with the Taylor series expansion of the dispersion function $\omega(\beta)$ and $z' = z - v_f t$. In the considered moving frame (t, z') , the front does not move and thus, represents a stationary perturbation, where the frequency of the signal $A(t, z')$ is not changed upon interaction. Thus, the interaction with the front can be well understood in this corrected frame as a signal propagating in the waveguide with a dispersion relation $\omega'(\beta) = \omega(\beta) - v_f \cdot (\beta - \beta_0)$ incident on an adiabatic perturbation that shifts the dispersion relation by $\Delta\omega_D(z')$.

To simulate signal propagation close to the band edge, we solve Eq. (1) by the split-step Fourier method,⁴⁰ where the additional

phase due to dispersion is calculated in the Fourier space and due to the perturbation in the real space. After the interaction with the front we like to convert the obtained spatial profile into the temporal profile to discuss the time sequence.³⁹ In order to calculate the temporal profile of the signal at any position z_0 , we Fourier transform the spatial profile of the signal $A(t_0, z)$ at any time t_0 into the spatial frequency domain $\tilde{A}_z(t_0, \beta)$. Using the dispersion relation $\omega(\beta)$, we calculate the frequency spectral power $|\tilde{B}_t(\omega, z_0)|^2 = |\tilde{A}_t(t_0, \beta(\omega))|^2 / v_g(\omega)$ at $z = z_0$, where v_g is the signal group velocity. The complex spatial frequency amplitudes, known at time t_0 , are multiplied with an additional phase shift $e^{i(\omega \cdot t_0 + \beta(\omega) \cdot z_0)}$ in order to get the correct phase of the temporal frequency amplitudes at position z_0 . Finally, we inverse Fourier transform the frequency components to obtain the temporal envelope of the signal pulse $B(t, z_0)$ at position z_0 .

For the propagating index front, we neglect the action of the signal on this front. In addition, we make an assumption that the front propagates with a constant velocity v_f and does not change during the propagation. This idealized representation is chosen to simplify the system and to highlight the front interactions without additional effects. To obtain such a situation, the pump should be positioned in the straight section of the dispersion curve or fulfill a soliton condition.⁴⁰ There are two other alternative descriptions of the nonlinear periodical waveguides. One includes the consideration of nonlinear coupled equations for forward and backward propagating plane waves without dispersion,^{41–43} while the other models the propagation in the periodic media by nonlinear Bloch modes.⁴⁴ We use the second description that requires only one equation with the inclusion of the dispersion. Similar results can also be obtained with the finite-difference time-domain (FDTD) method.^{45,46}

Here, we consider an example for light at $1.55 \mu\text{m}$ in a waveguide with a hyperbolic dispersion relation $\omega(\beta) = \omega_{\text{PBG}} + \Delta\omega_{\text{PBG}} \cdot \sqrt{1 + [(\beta - \beta_{\text{PBG}})^2 / \Delta\beta_{\text{PBG}}^2]}$, emulating an upper branch of a dispersion relation with a photonic bandgap (PBG), employing a PBG half opening of $\Delta\omega_{\text{PBG}} = 2.5 \text{ THz}$ and a PBG center frequency of $\omega_{\text{PBG}} = 197.5 \text{ THz}$ [cf. Fig. 1(a)]. $\Delta\beta_{\text{PBG}} = \Delta\omega_{\text{PBG}} / v_{g\infty}$ is the parameter that is chosen in such a way that away from the band edge, the dispersion relation converges to a straight line with a group velocity of $v_{g\infty} = c/2$. Here, β_{PBG} is the center wavenumber of the PBG, and c is the velocity of light in vacuum. The band diagram shift induced by the front is described by the function $\Delta\omega_D(t) = \Delta\omega_{\text{Dmax}}/2 \cdot [1 + \tanh(1/\Delta t_f(t - z/v_f))]$, where $\Delta t_f = 1 \text{ ps}$ is the temporal front width and $\Delta\omega_{\text{Dmax}} = 1 \text{ THz}$ is the maximum vertical band diagram shift in frequency, cf. dashed black curve in Fig. 1(a).

A. Pulse time reversal

As discussed before, the angle of the indirect transition induced by the moving index front is defined by the velocity of the front. Figure 1(a) shows a schematic representation of different free carrier front-induced indirect transitions in a highly dispersive system with a hyperbolic dispersion as an example. The hyperbolic dispersion is a good approximation for the dispersion of a weak Bragg grating in an otherwise dispersionless waveguide.⁴⁷ In addition, this kind of dispersion relation appears in periodic structures, such as photonic crystal waveguides,⁴⁸ photonic crystal fibers,⁴⁹ fiber Bragg gratings,^{47,50} and silicon and silicon nitride Bragg gratings.^{51,52} In

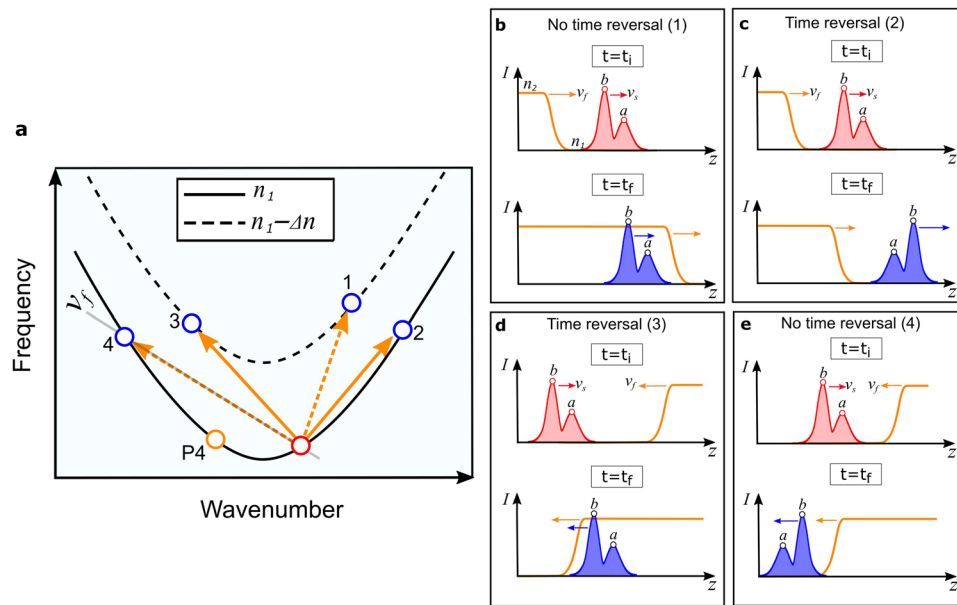


FIG. 1. (a) Schematic representation of different indirect transitions in a highly dispersive dispersion relation by changing the front velocity only. The solid curve represents the dispersion bands of an original (unperturbed) mode, while the dashed curves indicate the switched (perturbed) state. Red and blue circles indicate the initial and final states of the signal wave, respectively. Transitions 1 and 3: transmission through co/counter-propagating front (inter-band transitions) without/with time reversal, respectively. Transitions 2 and 4: reflection from a co/counter-propagating front (intra-band transitions) with/without time reversal, respectively. The gray line represents the phase continuity line with a slope equal to the group velocity of the front (we show only one line in Case 4 for clarity). P4 denotes the position of the pump/front on the band diagram corresponding to transition 4. [(b)–(e)] Schematic representation of the interaction between the signal and the front at two different times in the case of time reversal (corresponding to transitions 2 and 3) and no time reversal (corresponding to transitions 1 and 4). Red and blue arrows represent the propagation directions and group velocities of the signal before and after the interaction, respectively, while the orange arrow is for the index front. t_i and t_f are initial and final times, respectively.

this schematic example, the solid curve represents the dispersion band of an original (unperturbed) mode, while the dashed curve indicates the switched (perturbed) state after the front. The red and blue circles indicate the initial and final states of the signal wave, respectively. Here, the initial group velocities of the front (indicated by the slope of the orange arrow) and of the signal are co-directed for transitions 1 and 2, while they are counter-directed in transitions 3 and 4. The front group velocity can be tuned with respect to the signal by tuning the pump frequency on the dispersion relation, and thus the corresponding group velocity. The orange circle represents the position of the pump/index front on the dispersion relation corresponding to transition 4, and the gray line represents the corresponding phase continuity line with a slope equal to the group velocity of the index front (we show only one pump position and one line corresponding to transition 4 for clarity). In particular, we can position the pump on the other branch of the hyperbolic dispersion curve close to PBG to avoid the frequency overlap with the signal. Transitions 1 and 3 correspond to interband transitions, where final states are those of the perturbed waveguide and, thus, the signal transmits through the front,^{30,31} while transitions 2 and 4 are intraband transitions with reflection from the front in the forward^{27,32,38,53} and backward directions,⁴⁶ correspondingly.

As we mentioned before, time reversal means that the time order of an incident signal pulse is reversed, i.e., the leading edge

becomes the trailing edge and vice versa, after transition. To obtain that, the spatial sequential order of the signal pulse or its group velocity should be reversed but not both. That is the main condition apart from the profiles of the photonic band and refractive index front. Ideally, the time inversion should reproduce the envelope function $A(t, z_i)$ at some other location z_f and time t_f after the transition with negative time $A(t_f - t, z_f)$. In this work, we demonstrate the time reversal by changing the sequence of pulses in time. There is also a slight distortion and compression of signals that we discuss separately. With that the transitions 2 and 3 lead to time reversal and transitions 1 and 4 do not. Transition 3 is a transmission reversal, where the final state of the signal pulse is after interaction with the front is behind the front with the same spatial order but with the opposite group velocity to its initial state; thus, the time reversal is observed. Alternatively, forward reflection from a co-propagating front (transition 2) can also be used for signal reversal as in the optical analog of event horizons.^{27,33,38} In this case, the reflected signal does not change its propagation direction but its trailing edge interacts with the front first and becomes the leading edge after reflection, thus reversing the spatial order. Figures 1(b)–1(e) schematically demonstrate the interaction between the signal and the front at two different times in the case of time reversal (corresponding to transitions 2 and 3) and no time reversal (corresponding to transitions 1 and 4). Red and blue arrows represent the propagation directions and the corresponding group velocities of the

signal before and after the interaction, respectively, while the orange arrow demonstrates the front velocity. In the case of transition 3, after interaction with the front, the signal changes its propagation direction while keeping its spatial order; thus, the leading edge of the signal becomes the trailing edge and time reversal occurs. While in the case of transition 4, although the signal changes its direction after reflection from the counter-propagating front, no time reversal happens, as the signal also changes its space order. It is worth mentioning that the pulse time reversal needs a precise control of the front. The front velocity defines the transition direction, and it can be precisely tuned by the frequency of the pump, and thus, choosing its position and group velocity on the dispersion relation. The final frequency distribution of the signal is independent of the front shape, which is the case for all complete indirect transitions.²⁵ On the other hand, the penetration depth into the front is frequency dependent; thus, a time delay between the frequency components is accumulated leading to additional signal dispersion. Therefore, sharper fronts are better to avoid large delay difference. Additionally, in the case of interband transitions, the final dispersion curve is defined by the strength of the front. Thus, for the intraband transition 2, the final dispersion is front strength independent, as the converted signal stays on the original dispersion curve. Transition 3, however, is strength dependent.

Simulation results corresponding to the scenarios 1–4 in Fig. 1(a) are presented in Fig. 2. The temporal evolutions of a double Gaussian signal pulse with a duration of 100 ps and a velocity of $c/7$ using Eq. (1) represented in the stationary frame are shown in Figs. 2(a), 2(c), 2(e), and 2(g), respectively. The pseudo color indicates the power of the signal pulse. The dashed orange line marks the center of the index front. The corresponding temporal profiles of the input (red curve) and the output (blue curve) of the signal pulses are presented in Figs. 2(b), 2(d), 2(f), and 2(h), respectively. As we can see, for transitions 1 and 4, there is no time reversal, while we have time reversal for transitions 2 and 3. In the considered hyperbolic dispersion relation (see Sec. II), all group velocities of the index front between $c/2$ and zero can be obtained by tuning the pump frequency on the dispersion relation. The front velocity in the case of transition 1 ($c/1.3$) is chosen for schematic presentation purposes only and cannot be excited using the proposed dispersion relation. The signal pulse after interaction with the front also experiences a temporal and a spatial compression. The frequency width of the final state of the signal pulse increases. This can be explained schematically by projecting the initial frequency width, via the phase continuity lines [gray line in Fig. 1(a)], on the perturbed/unperturbed dispersion relation.⁴⁵ From this geometrical consideration, the temporal compression factor $t_{\text{input}}/t_{\text{output}}$ can be derived as $[(1 - v_f/v_{g1})/(v_f/v_{g2} - 1)]$, where v_{g1} and v_{g2} are the group velocities of the signal before and after the interaction with the front. Provided that the phase continuity line does not cut through the perturbed dispersion function, the compression factor increases when the front velocity approaches the slope of the dispersion relation away from the band edge $c/2$, as then the frequency bandwidth of the converted signal becomes maximal.³⁹ However, the pulse compression can be avoided in the case of transition 3, if signal group velocities and front velocity are correctly adjusted.

We can also see some distortion in the output pulse in Fig. 2(f) due to the dispersion. First, all the signals propagate in the dispersive waveguide before and after the transition. Also, the penetration

depth into the front is frequency dependent, and thus, additional time delay difference is accumulated. Such dispersion can be compensated by additional measures. Alternatively, a waveguide with piecewise linear dispersion should be used and the fronts should be sharp to avoid a large delay difference.

Our considerations of transmission through the front disregard the partial reflections. The front is much longer than the wavelength of the incident signal wave, and the non-adiabatic, Fresnel-like reflection from the index front can be ignored. This is a typical situation for fronts excited by pump pulses. Furthermore, front-induced adiabatic transmission or reflection leads in a lossless case to 100% conversion efficiency. Losses diminish the efficiency as observed in Ref. 38.

One of the advantages of front-induced time reversal is the capability to reverse any input pulse shape as well as multiple pulses (package of information) in only one step. Simulation results of time reversal of pulse with 5 peaks is presented in Fig. 3.

B. Light stopping/storage and releasing

Light stopping and releasing can be also realized in waveguides by inducing indirect photonic transitions to a point of zero group velocity (Fig. 4, blue circle). This approach is experimentally more feasible than the band tilting in a direct transition.^{14,18,19} Strong band tilting requires local refractive index variations that are difficult to realize.¹⁴ The mechanism of signal releasing is also important. In the case of fronts, backward transition can be obtained by a front with the same velocity but an opposite slope. Front-induced pulse stopping can be achieved via interaction with either a free-carrier or Kerr-induced index fronts. The advantage of the free-carrier front is the possibility to keep the system in the switched state for a comparatively long time, which is defined by the free carrier life time in the waveguide in the order of nanoseconds.^{15,20} In the case of the free-carrier index front, the storage is possible via transmission through either a counter- (cf. transition 1 in Fig. 4) or co-propagating (cf. transition 3 in Fig. 4) index front, or via reflection from the leading edge of a co-propagating front (cf. transition 2 in Fig. 4). However, the stored signal is attenuated by the free-carrier absorption. In order to obtain a front of opposite sign, which corresponds to a controlled depletion of free carriers, a reverse bias can be applied in a PIN-junction-loaded waveguide.⁵⁴ However, in this case, the carrier decay becomes much faster and the rectangular pump pulse is required to maintain free carrier concentrations for the required storage time. A Kerr nonlinearity without significant two photon absorption^{55,56} is more promising for storage. In the case of a Kerr-induced front, a signal pulse can be stored/released via the reflection from the trailing/leading edge of the pump pulse [Figs. 4(c) and 4(d)]. Storage can also be obtained by transmission either through the trailing edge or through the leading edge of the Kerr-induced front. Storage by transmission through the trailing edge Kerr front is only possible for signal pulses that are initially temporally inside the pump pulse. In this case, the signal stops after coming out of the pump pulse through the trailing edge and can be released and collected by the leading edge of the successive pulse. However, in this configuration, the initial signal duration should be shorter than the pump pulse. On the other hand, the stopping by the transmission through the leading edge of the pump pulse is not useful as the stopped signal would right away encounter an opposite slope of the

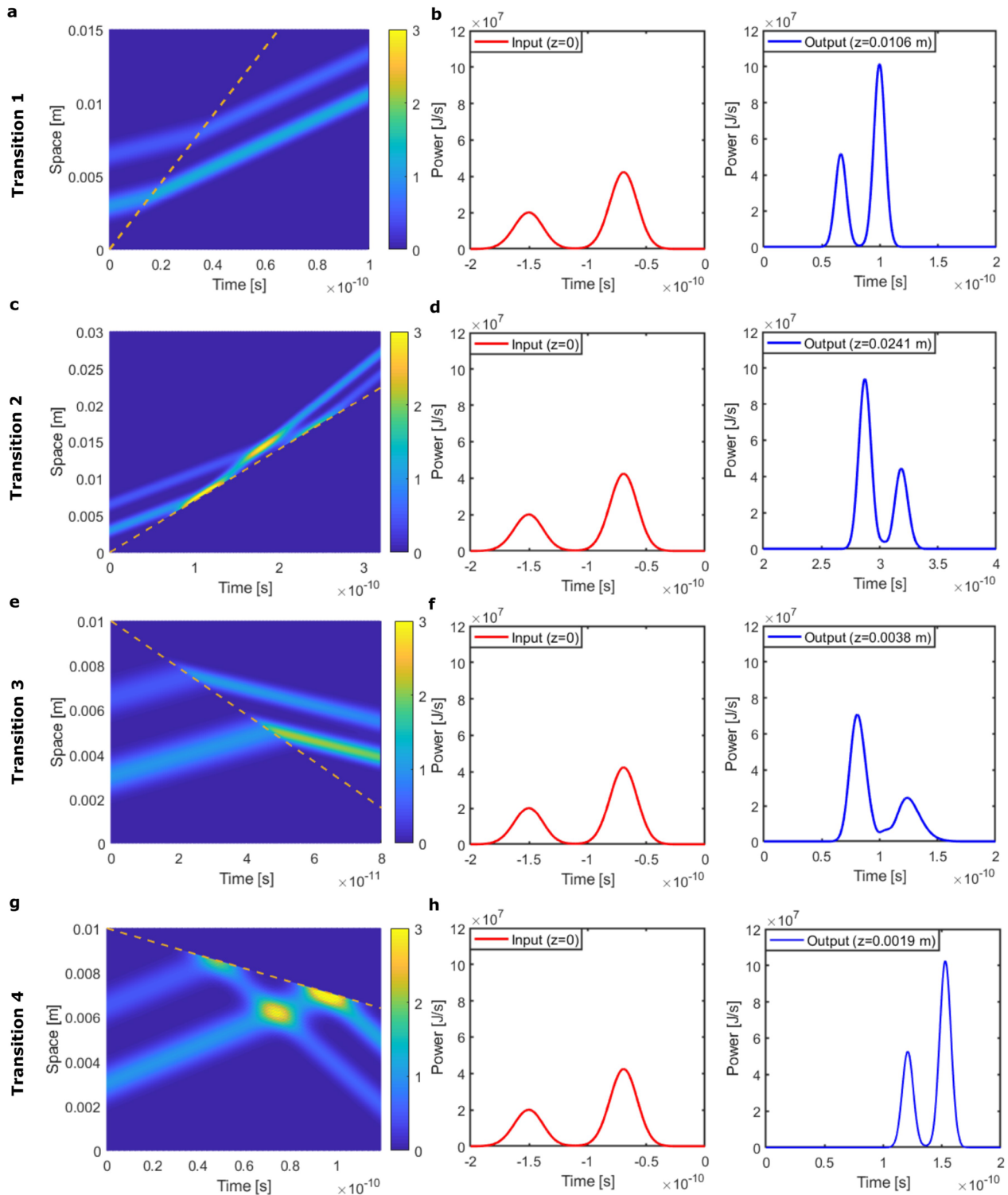


FIG. 2. (a), (c), (e), and (g) Temporal evolution of the signal represented in the stationary frame cf. transitions 1, 2, 3, and 4 in Fig. 1(a), respectively. The velocity ($c/7$) and duration ($\tau_s = 100$ ps) of the input signal pulse are the same for all cases. However, the velocities of the index fronts are $c/1.3$, $c/4.28$, $-c/2.85$, and $-c/10$ in the cases of (a), (c), (e), and (g), respectively. The pseudo color indicates the linear energy density of the signal. (b), (d), (f), and (h) The corresponding input (red curve) and output (blue curve) temporal profiles of the signal.

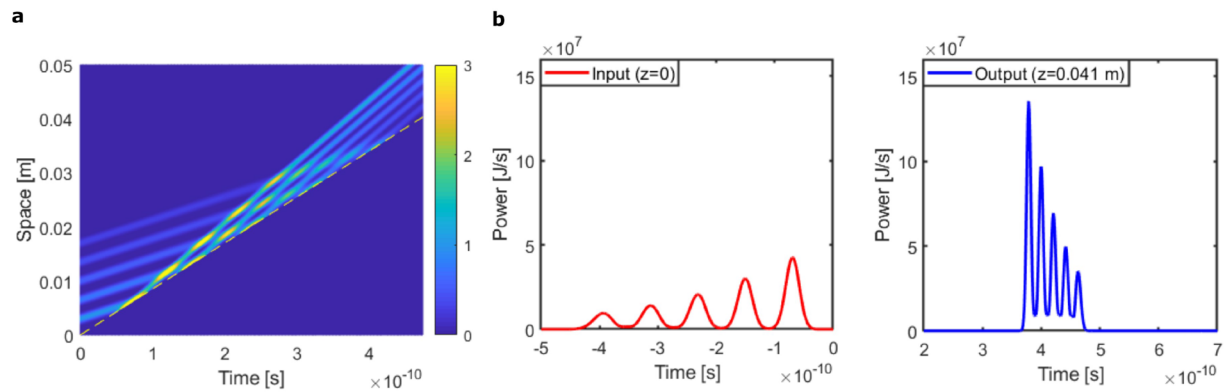


FIG. 3. Simulation results of time reversal for a multi-peaks signal pulse. (a) Temporal evolution of the signal represented in the stationary frame cf. transition 2 in Fig. 1(a). The pseudo color indicates the linear energy density of the signal. (b) The input (red curve) and output (blue curve) temporal profiles of the signal.

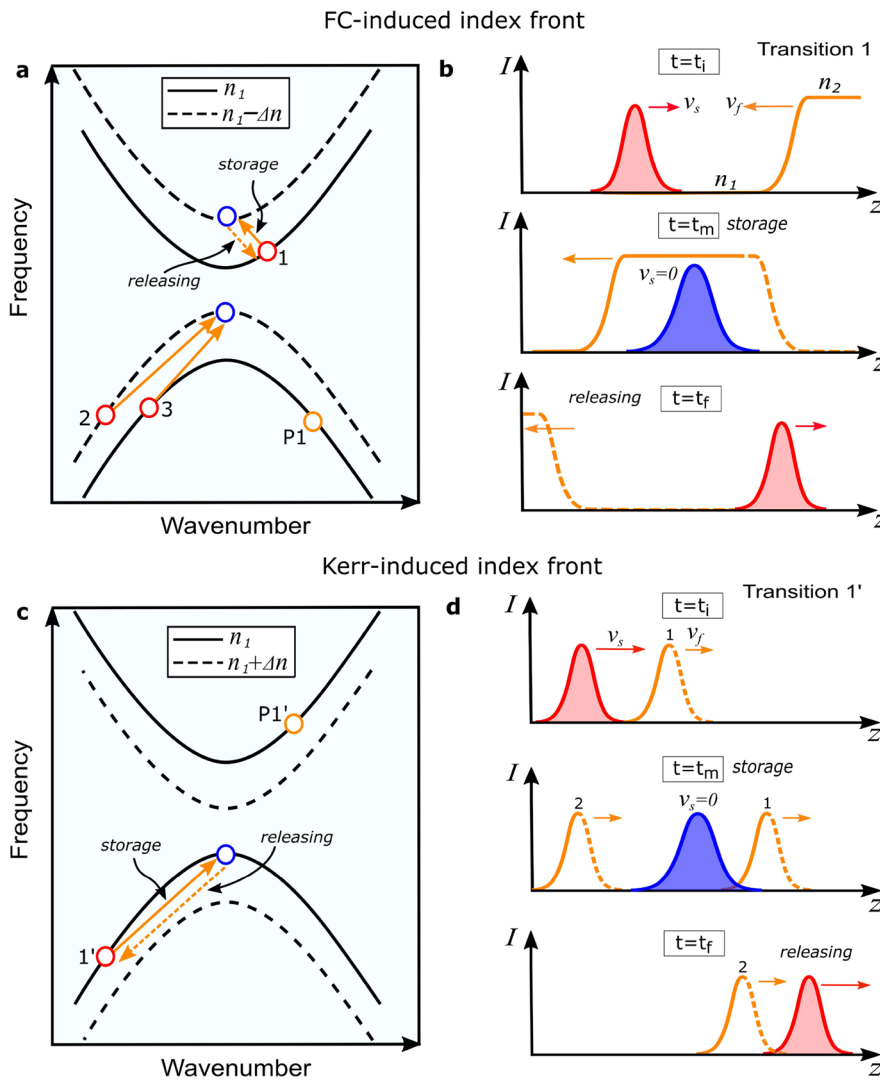


FIG. 4. Schematic representation of different front-induced light stopping schemes. (a) Pulse stopping can be achieved via interaction with a free-carrier-induced index front. Storage is possible in this case via transmission through either a counter- (transition 1) or co-propagating (transition 3) index front, or via reflection from the leading edge of a co-propagating front (transition 2). The signal can be later released by the front with an opposite slope. The solid orange arrow in transition 1 denotes the stopping-related transition, while the dashed orange arrow denotes the releasing transition. P1 denotes the position of the pump/front in the band diagram corresponding to transition 1. (b) Schematic representation of the signal stopping and releasing process in the case of transition 1. t_i , t_m , and t_f are initial, middle, and final times, respectively. (c) Kerr-induced signal stopping and releasing. The signal pulse is stored after reflection from the trailing edge of the Kerr-induced perturbation, and then can be released via the reflection from the leading edge of the second pulse. P1' denotes the position of the pump/front in the band diagram corresponding to transition 1'. This mechanism can be realized, for example, inside a silicon-rich nitride waveguides. These waveguides have a high nonlinear parameter ($550 \text{ W}^{-1}/\text{m}$),⁵⁵ therefore, a 100 W on-chip pump peak power at $1.5 \mu\text{m}$ wavelength can lead to a sufficient Kerr modulation ($\Delta n \approx 0.01$) that is required to induce a band shift in the order of 1 THz. (d) Representation of the Kerr-induced signal stopping and releasing (cf. transition 1').

trailing edge, thus would be released. We have to mention that Kerr-induced self-phase-modulation (SPM) causes a temporally varying instantaneous frequency. In this way, an initial non-chirped pump pulse acquires a frequency chirp. Still this frequency chirp does not change the pulse envelope, thus, the front shape if the pump propagates in the waveguide with negligible dispersion. Schematic representations of signal storage and release by transmission through a free-carrier (cf. transition 1 in Fig. 4) and reflection from Kerr (cf. transition 1' in Fig. 4) fronts at different times are shown in Figs. 4(b) and 4(d), respectively. In the case of reflection-induced storage from the Kerr front [Fig. 4(d)], the faster signal pulse in its initial position (red circle) does not see the leading edge of Pulse 1 but only the trailing edge, as this interaction moves the signal in the new state (stopped) along the solid orange arrow direction. Later, the stopped signal (blue circle) is released by reflection in the forward direction from the leading edge of Pulse 2 along the dashed arrow. In this case, the signal is gone from the stopping position in the band diagram before it sees the trailing edge of the front. To our knowledge, the aforementioned storage mechanisms have not been realized so far.

It should be mentioned that depending on the initial bandwidth of the signal, on the dispersion at the zero group velocity point, and on the slope of the indirect transition, the final signal has some frequency components at non-zero group velocities. Thus, with time,

the stored signal disperses in forward and backward directions and leaves the structure. Therefore, the limits of the storage time in this case are defined by the curvature of the dispersion relation at the zero group velocity. In any case, the maximal storage time is obtained if the spatial pulse envelope of the stopped signal is close to the waveguide length. In this case, minimal bandwidths of spatial frequencies are excited.

In the case of a hyperbolic dispersion relation, if the wave number bandwidth $\Delta\beta$ of the initial signal lies on the straight section of the dispersion relation, the initial signal dispersion is negligible. In addition, the signal dispersion during the interaction with the front or during the writing time can be neglected if the storage time of the signal is much larger than the propagation time of the front inside the waveguide. Therefore, as soon as the signal is stored/written in the waveguide, the only factors that determine the storage time are the final wave number bandwidth $\Delta\beta'$ of the signal and the dispersion at the band edge, as we mentioned before. Interesting is that keeping $\Delta\beta'$ constant and by increasing the front velocity, and therefore the slope of the phase continuity line, we can project the final frequency bandwidth $\Delta\omega'$ from a very broad initial frequency bandwidth $\Delta\omega$ on the dispersion relation, provided that the phase continuity line can reach the final state on the same band without cutting into the shifted band. Thus, we can store input signals with

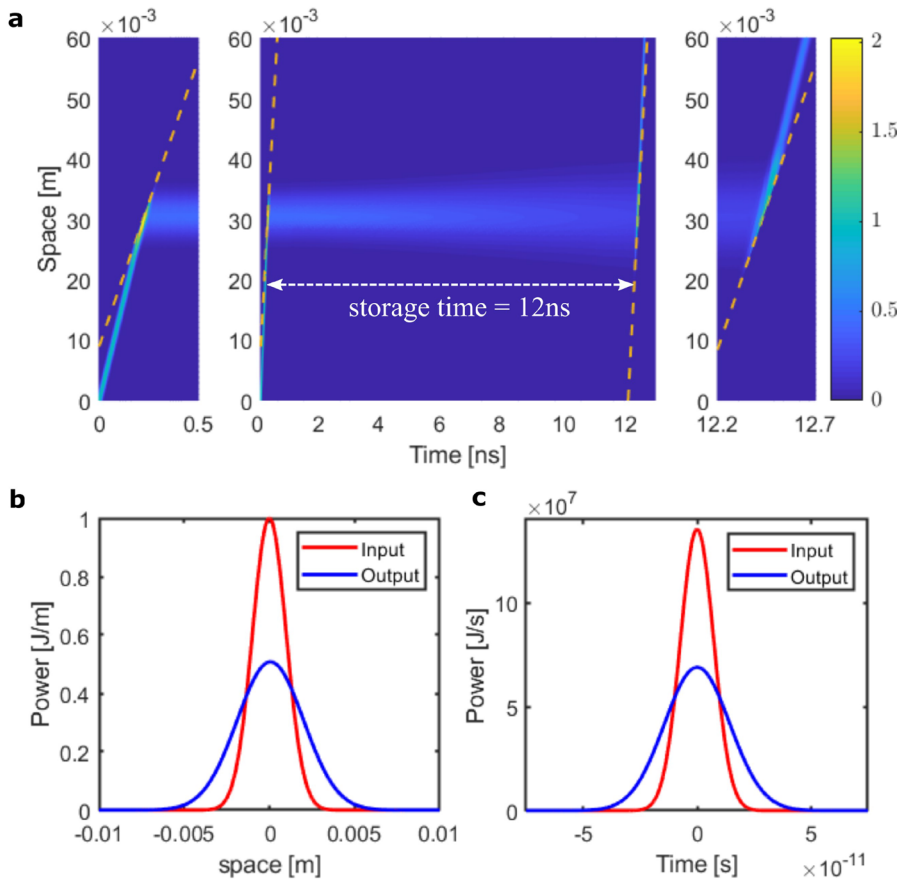


FIG. 5. Simulation of signal stopping and releasing: (a) Temporal evolution of the signal represented in the stationary frame cf. transition 1' in Fig. 4(c). The velocity of the input signal is $c/2.2$, while that of the index fronts is $c/3.16$. The pseudo color indicates the intensity of the electric field of the signal. The signal is first stopped via the front with a negative slope (left dashed orange line), and then is released by a second front with a positive slope (right dashed orange line). Zoom in views of signal reflection from the negative/positive fronts are presented in left/right panels. The corresponding input (red curve) and output (blue curve) spatial and temporal envelopes of the signal are shown in (b) and (c), respectively.

different temporal bandwidths into a stopped signal with the same spatial width and spatial frequency, and thus, store it for the same time inside the waveguide.

Figure 5 shows the simulation results of signal pulse stopping and releasing via the reflection from co-propagating index fronts with opposite slopes [cf. transition 1' in Fig. 4(c)]. Here, the initial signal pulse has a duration of $\tau_s = 20$ ps, a width of $z_s = 5$ mm, and a velocity of $v_s = c/2.2$, while the front duration is $\tau_f = 1$ ps and the front velocity is $v_f = c/3.16$. The temporal evolution of the signal pulse spatial envelope in the stationary frame is represented in Fig. 5(a). It is shown that in the stationary frame, the signal pulse is recorded in space after reflection from the trailing edge of the slower index front. As not all frequency components of the initial signal are stopped due to the curvature of the dispersion relation around zero group velocity, the stopped signal disperses over time. A second front with an opposite slope then releases the stopped signal, converting it back to the propagation mode. Figures 5(b) and 5(c) show the spatial and temporal envelopes of the input (red curve) and output (blue curve) signal pulses, respectively. We define here the storage time as the time at which the full width at half maximum (FWHM) of the output spatial or temporal envelopes is doubled compared to the input signal z_s . The maximum storage time that can be obtained inside a 1 cm waveguide is ~ 12 ns for the dispersion parameters under consideration. We have to mention that the presented results are experimentally feasible using existing photonic waveguide technologies. For example, the band shift of 1 THz used here in the simulation can be obtained experimentally in ultra-silicon-rich nitride (Si_7N_3) waveguides that have a high nonlinear parameter of $550 \text{ W}^{-1}/\text{m}$.⁵⁵ Assuming a 100 W on-chip pump peak power at $1.5 \mu\text{m}$ wavelength, this leads to a refractive index modulation in the waveguide of $\Delta n \approx 0.01$ and accordingly a maximal band shift of $\Delta\omega_{\text{Dmax}} \approx 1$ THz. In addition, waveguides made from III-V semiconductors such as GaInP could be another candidate due to their high nonlinear parameter (ranging from $\sim 500 \text{ W}^{-1}/\text{m}$ to $2900 \text{ W}^{-1}/\text{m}$) and the absence of two photon absorption at $1.5 \mu\text{m}$.^{57–59}

Waveguide imperfections result in propagation loss α_z due to vertical scattering that scales with $\alpha_z \sim 1/v_g$.⁶⁰ However, in the case of storage, we should consider the loss per time α_t , i.e., $\alpha_t = \alpha_z \cdot v_g \sim 1/v_g \cdot v_g$, which is group velocity independent. To make a lower estimate of the loss, we can consider the standing wave as a coupled state of forward and backward propagating waves.^{41,42} In a structure with disorder, these waves lose energy proportional to the time spent in the structure, irrespective of the fact if they are coupled to each other or not. A waveguide loss of ~ 1 dB/cm with $n_g = 3$ corresponds to the propagation of 10 cm in 1 ns or a loss of 10 dB per 1 ns. If propagation losses are reduced below 0.1 dB/cm,^{61,62} then losses not bigger than 1 dB/ns should be expected.

III. CONCLUSIONS

We have shown a scheme for dynamic pulse time reversal and stopping in optical waveguide systems via indirect FITs. We used the linear Schrödinger equation, where the temporal evolution of the pulse spatial profile is tracked to simulate these transitions. In contrast to other schemes, pulse time reversal/stopping via FITs are not limited by a strict phase matching condition, and thus, broadband signals can be time reversed/stopped even in non-parallel and

curved dispersion bands. Furthermore, this scheme does not require the complex local modulation of the refractive index and the simple nonlinear switching pulse propagating through the waveguide can induce the required transition of the signal. In addition, pulse time reversal and stopping in a reflection mode need precise control of the front velocity only, however, they are independent of the front shape.

Two optical transitions are identified that lead to time reversal. One of them corresponds to the transmission through the front with a corresponding change in the group velocity sign. In this case, the signal keeps its spatial sequence but reverses its propagation direction. Another transition corresponds to signal forward reflection from a co-propagating front. In this case, the group velocity sign is the same but the spatial sequence is reversed. Both transitions can be realized experimentally. The optical analog of the event horizon with the corresponding forward reflection from the front²⁷ also leads to such transitions. At the same time, the FIT produces the time reversed signal that can be different in duration, compressed or broadened, and can be slightly distorted by dispersion. Both effects can be avoided by the adjustment of the dispersion relation.

Several possibilities are identified for light stopping by FIT with free-carrier and Kerr-induced fronts. Advantageous is the signal stopping by the reflection from the trailing edge of the pulse with Kerr-nonlinearity and releasing by the second reflection from the leading edge of the second pulse. Such a scheme allows light storage in the unperturbed waveguide. We show that even in the periodic waveguide with strong dispersion close to the band edge storage times in the order of 10 ns in 1 cm waveguide are feasible. In real systems, the effects of the linear/scattering losses at the band edge limits the storage time of the pulse.

ACKNOWLEDGMENTS

The authors acknowledge the support from the German Research Foundation (DFG) (Grant No. 392102174) as well as Dassault Systemes with their CST Studio Suite software. We further acknowledge support for the Open Access fees by Hamburg University of Technology (TUHH) in the funding programme Open Access Publishing.

DATA AVAILABILITY

The data that support the findings of this study are available from the corresponding author upon reasonable request.

REFERENCES

- ¹A. E. Willner, S. Khaleghi, M. R. Chitgarha, and O. F. Yilmaz, *J. Lightwave Technol.* **32**, 660 (2014).
- ²S. Wengerowsky, S. K. Joshi, F. Steinlechner, H. Hübel, and R. Ursin, *Nature* **564**, 225 (2018).
- ³D. Marom, D. Panasenkov, R. Rokitski, P.-C. Sun, and Y. Fainman, *Opt. Lett.* **25**, 132 (2000).
- ⁴O. Kuzucu, Y. Okawachi, R. Salem, M. A. Foster, A. C. Turner-Foster, M. Lipson, and A. L. Gaeta, *Opt. Express* **17**, 20605 (2009).
- ⁵A. V. Chumak, V. S. Tiberkevich, A. D. Karenowska, A. A. Serga, J. F. Gregg, A. N. Slavin, and B. Hillebrands, *Nat. Commun.* **1**, 141 (2010).
- ⁶L. Yuan, M. Xiao, and S. Fan, *Phys. Rev. B* **94**, 140303 (2016).
- ⁷M. F. Yanik and S. Fan, *Phys. Rev. Lett.* **93**, 173903 (2004).

- ⁸S. Longhi, *Phys. Rev. E* **75**, 026606 (2007).
- ⁹Y. Sivan and J. B. Pendry, *Phys. Rev. Lett.* **106**, 193902 (2011).
- ¹⁰M. Minkov and S. Fan, *Phys. Rev. B* **97**, 060301 (2018).
- ¹¹R. Konoike, T. Asano, and S. Noda, *APL Photonics* **4**, 030806 (2019).
- ¹²M. F. Yanik and S. Fan, *Phys. Rev. Lett.* **92**, 083901 (2004).
- ¹³Y. Saito and T. Baba, *Opt. Express* **18**, 17141 (2010).
- ¹⁴D. M. Beggs, T. F. Krauss, L. Kuipers, and T. Kampfrath, *Phys. Rev. Lett.* **108**, 033902 (2012).
- ¹⁵K. Kondo, M. Shinkawa, Y. Hamachi, Y. Saito, Y. Arita, and T. Baba, *Phys. Rev. Lett.* **110**, 053902 (2013).
- ¹⁶T. Baba, *Nat. Photonics* **2**, 465 (2008).
- ¹⁷T. F. Krauss, *Nat. Photonics* **2**, 448 (2008).
- ¹⁸M. F. Yanik and S. Fan, *Phys. Rev. A* **71**, 013803 (2005).
- ¹⁹M. C. Munoz, A. Kanchana, A. Y. Petrov, and M. Eich, *IEEE J. Quantum Electron.* **48**, 862 (2012).
- ²⁰Q. Xu, P. Dong, and M. Lipson, *Nat. Phys.* **3**, 406 (2007).
- ²¹Y. Tanaka, J. Upham, T. Nagashima, T. Sugiya, T. Asano, and S. Noda, *Nat. Mater.* **6**, 862 (2007).
- ²²T. Tanabe, M. Notomi, E. Kuramochi, A. Shinya, and H. Taniyama, *Nat. Photonics* **1**, 49 (2006).
- ²³A. W. Elshaari, A. Aboketaf, and S. F. Preble, *Opt. Express* **18**, 3014 (2010).
- ²⁴J. Upham, Y. Fujita, Y. Kawamoto, Y. Tanaka, B. S. Song, T. Asano, and S. Noda, *Opt. Express* **21**, 3809 (2013).
- ²⁵M. A. Gaafar, T. Baba, M. Eich, and A. Y. Petrov, *Nat. Photonics* **13**, 737 (2019).
- ²⁶R. Dekker, A. Driessen, T. Wahlbrink, C. Moormann, J. Niehusmann, and M. Först, *Opt. Express* **14**, 8336 (2006).
- ²⁷T. G. Philbin, C. Kuklewicz, S. Robertson, S. Hill, F. König, and U. Leonhardt, *Science* **319**, 1367 (2008).
- ²⁸V. E. Lobanov and A. P. Sukhorukov, *Phys. Rev. A* **82**, 033809 (2010).
- ²⁹A. P. Sukhorukov, T. A. Voitova, V. E. Lobanov, A. N. Bugai, and S. V. Sazonov, *Bull. Russ. Acad. Sci.: Phys.* **76**, 305 (2012).
- ³⁰M. Castellanos Muñoz, A. Y. Petrov, L. O'Faolain, J. Li, T. F. Krauss, and M. Eich, *Phys. Rev. Lett.* **112**, 053904 (2014).
- ³¹K. Kondo and T. Baba, *Phys. Rev. Lett.* **112**, 223904 (2014).
- ³²B. W. Plansinis, W. R. Donaldson, and G. P. Agrawal, *Phys. Rev. Lett.* **115**, 183901 (2015).
- ³³C. Ciret, F. Leo, B. Kuyken, G. Roelkens, and S.-P. Gorza, *Opt. Express* **24**, 114 (2016).
- ³⁴P. Kanakis and T. Kamalakis, *Opt. Lett.* **41**, 1372 (2016).
- ³⁵K. Kondo, N. Ishikura, T. Tamura, and T. Baba, *Phys. Rev. A* **91**, 023831 (2015).
- ³⁶M. A. Gaafar, A. Y. Petrov, and M. Eich, *ACS Photonics* **4**, 2751 (2017).
- ³⁷T. Marest, C. Mas Arabí, M. Conforti, A. Mussot, C. Milián, D. V. Skryabin, and A. Kudlinski, *Opt. Express* **26**, 23480 (2018).
- ³⁸M. A. Gaafar, D. Jalas, L. O'Faolain, J. Li, T. F. Krauss, A. Y. Petrov, and M. Eich, *Nat. Commun.* **9**, 1447 (2018).
- ³⁹M. A. Gaafar, H. Renner, A. Y. Petrov, and M. Eich, *Opt. Express* **27**, 21273 (2019).
- ⁴⁰G. Agrawal, *Nonlinear Fiber Optics*, 5th ed. (Academic Press, 2013).
- ⁴¹J. E. Sipe and H. G. Winful, *Opt. Lett.* **13**, 132 (1988).
- ⁴²C. M. de Sterke, *Opt. Lett.* **17**, 914 (1992).
- ⁴³B. J. Eggleton, R. E. Slusher, C. M. de Sterke, P. A. Krug, and J. E. Sipe, *Phys. Rev. Lett.* **76**, 1627 (1996).
- ⁴⁴N. A. R. Bhat and J. E. Sipe, *Phys. Rev. E* **64**, 056604 (2001).
- ⁴⁵E. A. Ulchenko, D. Jalas, A. Y. Petrov, M. C. Muñoz, S. Lang, and M. Eich, *Opt. Express* **22**, 13280 (2014).
- ⁴⁶K. Kondo and T. Baba, *Phys. Rev. A* **93**, 011802 (2016).
- ⁴⁷C. M. de Sterke, N. G. R. Broderick, B. J. Eggleton, and M. J. Steel, *Opt. Fiber Technol.* **2**, 253 (1996).
- ⁴⁸J. Li, T. P. White, L. O'Faolain, A. Gomez-Iglesias, and T. F. Krauss, *Opt. Express* **16**, 6227 (2008).
- ⁴⁹J. M. Dudley, G. Genty, and S. Coen, *Rev. Mod. Phys.* **78**, 1135 (2006).
- ⁵⁰G. Meltz, W. W. Morey, and W. H. Glenn, *Opt. Lett.* **14**, 823 (1989).
- ⁵¹M. Verbist, W. Bogaerts, and D. van Thourhout, *J. Lightwave Technol.* **32**, 1915 (2014).
- ⁵²E. Sahin, A. Blanco-Redondo, P. Xing, D. K. T. Ng, C. E. Png, D. T. H. Tan, and B. J. Eggleton, *Laser Photonics Rev.* **13**, 1900114 (2019).
- ⁵³N. N. Rosanov, N. V. Vysotina, and A. N. Shatsev, *JETP Lett.* **93**, 308 (2011).
- ⁵⁴K. Kondo and T. Baba, *Phys. Rev. A* **97**, 033818 (2018).
- ⁵⁵T. Wang, D. K. T. Ng, S.-K. Ng, Y.-T. Toh, A. K. L. Chee, G. F. R. Chen, Q. Wang, and D. T. H. Tan, *Laser Photonics Rev.* **9**, 498 (2015).
- ⁵⁶H. El Dirani, A. Kamel, M. Casale, S. Kerdiles, C. Monat, X. Letartre, M. Pu, L. K. Oxenlowe, K. Yvind, and C. Sciancalepore, *Appl. Phys. Lett.* **113**, 081102 (2018).
- ⁵⁷P. Colman, C. Husko, S. Combrié, I. Sagnes, C. W. Wong, and A. de Rossi, *Nat. Photonics* **4**, 862 (2010).
- ⁵⁸U. D. Dave, B. Kuyken, F. Leo, S.-P. Gorza, S. Combrié, A. De Rossi, F. Raineri, and G. Roelkens, *Opt. Express* **23**, 4650 (2015).
- ⁵⁹V. Eckhouse, I. Cestier, G. Eisenstein, S. Combrié, P. Colman, A. de Rossi, M. Santagiustina, C. G. Someda, and G. Vadalà, *Opt. Lett.* **35**, 1440 (2010).
- ⁶⁰S. Hughes, L. Ramunno, J. F. Young, and J. E. Sipe, *Phys. Rev. Lett.* **94**, 033903 (2005).
- ⁶¹J. Cardenas, C. B. Poitras, J. T. Robinson, K. Preston, L. Chen, and M. Lipson, *Opt. Express* **17**, 4752 (2009).
- ⁶²G. Li, J. Yao, H. Thacker, A. Mekis, X. Zheng, I. Shubin, Y. Luo, J.-h. Lee, K. Raj, J. E. Cunningham, and A. V. Krishnamoorthy, *Opt. Express* **20**, 12035 (2012).